Advances in Water Resources xxx (2010) xxx–xxx

Contents lists available at ScienceDirect

Advances in Water Resources

journal homepage: www.elsevier.com/ locate/advwatres

Snow distribution from SSM/I and its relationships to the hydroclimatology of the Mackenzie River Basin, Canada

Jinjun Tong [a,b,*], Stephen J. Déry [c], Peter L. Jackson [c], Chris Derksen [d]

[a] Natural Resources and Environmental Studies, University of Northern British Columbia, Prince George, BC, Canada V2N 4Z9
[b] Department of Earth System Science, University of California, Irvine, CA, 92697, USA
[c] Environmental Science and Engineering Program, University of Northern British Columbia, Prince George, BC, Canada V2N 4Z9
[d] Climate Research Division, Environment Canada, Toronto, Ontario, Canada M3H 5T4

ARTICLE INFO

Article history:
Received 3 November 2009
Received in revised form 18 March 2010
Accepted 19 March 2010
Available online xxxx

Keywords:
Snow distribution
Microwave remote sensing
Hydroclimatology

ABSTRACT

The spatial and temporal distribution of snow cover extent (SCE) and snow water equivalent (SWE) play vital roles in the hydrology of northern watersheds. We apply remotely sensed Special Sensor Microwave Imager (SSM/I) data from 1988 to 2007 to explore the relationships between snow distribution and the hydroclimatology of the Mackenzie River Basin (MRB) of Canada and its major sub-basins. The Environment Canada (EC) algorithm is adopted to retrieve the SWE from SSM/I data. Moderate Resolution Imaging Spectroradiometer (MODIS) 8-day maximum snow cover extent products (MOD10A2) are used to estimate the different thresholds of retrieved SWE from SSM/I to classify the land cover as snow or no snow for various sub-basins in the MRB. The sub-basins have varying topography and hence different thresholds that range from 10 mm to 30 mm SWE. The accuracy of snow cover mapping based on the combination of several thresholds for the different sub-basins reaches ≈90%. The northern basins are found to have stronger linear relationships between the date on which snow cover fraction (SCF) reaches 50% or when SWE reaches 50% and mean air temperatures, than the southern basins. Correlation coefficients between SCF, SWE, and hydroclimatological variables show the new SCF products from SSM/I perform better than SWE from SSM/I to analyze the relationships with the regional hydroclimatology. Statistical models relating SCF and SWE to runoff indicate that the SCF and SWE from EC algorithms are able to predict the discharge in the early snow ablation seasons in northern watersheds.

1. Introduction

The spatial and temporal distribution of snow cover extent (SCE) and snow water equivalent (SWE) play a critical role in the hydrology of northern watersheds [11,12,14,21,44–46]. Climate change influences the process of snow accumulation and ablation significantly [2], with recent research indicating a significant decrease of snow during spring over North America and Eurasia in response to rising air temperatures [3,4,10,16,27,28,35,37]. Barnett et al. [2] project that an acceleration of the hydrological cycle due to global warming in snowmelt-dominated regions will cause earlier snowmelt and timing of maximum SWE that may lead to regional water shortages. The strong link between SCE, SWE, and river discharge has been investigated in different regions such as the large Siberian watersheds [44,45], the Upper Rio Grande River Basin [47], and in northern Canada [32,36,37,46].

Numerical modeling and remotely sensed snow data have been widely used for cold region hydrometeorological investigations [25,32]. For instance, the National Oceanic and Atmospheric Administration (NOAA) weekly snow data and Moderate Resolution Imaging Spectroradiometer (MODIS) snow products are used to explore snow distributions and their relationships with river discharge [39,40,42,44,45,47]. The modeled and observed snow data have also been used to assess the interaction between snow and hydroclimatology [14]. Passive microwave remote sensing is used to monitor the SWE based on the difference of brightness temperature (TB) between various channels [6,7,15,38]. The Environment Canada (EC) algorithm for SWE retrieval from SSM/I has been developed and evaluated for the Mackenzie River Basin (MRB) and in northern Manitoba based on snow depth (SD) observations [8,9]. However, no study has applied the EC algorithm for SSM/I to describe the relationships between SCE, SWE, and river discharge in the MRB. In the Canadian Arctic, which is composed mainly of barren tundra, land cover cells are classified as snow or no snow based on a remotely sensed retrieved SWE threshold of 1 mm [5,42]. In addition, the liquid water in wet snow, the grain size, and land cover also influence the microwave signal from the snowpack to over- or under-estimate the SWE [8,9,22]. Therefore, a single threshold of 1 mm for classification of snow or no

* Corresponding author. Department of Earth System Science, University of California, Irvine, CA, 92697, USA.
E-mail address: jinjunt@uci.edu (J. Tong).

0309-1708/$ – see front matter © 2010 Elsevier Ltd. All rights reserved.
doi:10.1016/j.advwatres.2010.03.009

snow for different regions may introduce large errors for the estimation of SCE. However, there is limited research to estimate the SWE thresholds to classify the cells as snow or no snow in more complex terrain.

In this study, different thresholds from 0 mm to 50 mm of SWE from SSM/I are used to classify the pixels as snow or no snow. To determine the optimal thresholds of remotely sensed SWE from SSM/I in different topography and land cover in various basins, snow cover maps from SSM/I are compared to the MODIS 8-day maximum snow cover extent products (MOD10A2), which have been found to be highly accurate in many different geographic regions [17,18,20,23,26,29,31,39,40,43,47]. To decrease the impacts of clouds in MOD10A2, a spatial filter method is utilized before being compared to the SSM/I snow cover maps. Then, the new SCF products from SSM/I and SWE from SSM/I are adopted to quantitatively analyze the relationships with the MRB hydroclimatology.

2. Research area

The MRB, which is the tenth largest river basin in the world by area, covers about 1.8 million km^2 of northwestern Canada. It is located between latitudes 52°N–70°N, and longitudes 103°W–140°W with a wide range of elevations and land cover types (Fig. 1). The MRB includes six major sub-basins: the Peel, Great Bear, Liard, Great Slave, Peace, and Athabasca watersheds, which respectively cover about 182, 598, 428, 668, 509, and 452 SSM/I Equal-Area Scalable Earth-Grid (EASE-Grid) points. The EASE-Grid includes a set of three equal-area projections: Northern Hemisphere, Southern Hemisphere, and global. Details of the map projection parameters are available through the National Snow and Ice Data Center (NSIDC) [http://nsidc.org/data/ease/ease_grid.html]. The elevation of the western part of the MRB reaches ≈3000 m above sea level; however, the eastern part of the MRB is at lower elevations than the western part. The average elevation of the MRB is about 630 m above sea level. The Peel and Great Bear sub-basins are mainly covered by sparse vegetation and tundra; however, the other sub-basins are mostly covered by coniferous forests. In the MRB, the open area, sparse vegetation, coniferous forests, and deciduous forests account for about 14%, 40%, 34%, and 12%, respectively of land cover types. The Mackenzie River system spans 4241 km from the Columbia Icefield in Jasper National Park to its mouth on the Beaufort Sea of the Arctic Ocean. The river discharge gauges in the MRB, Peel River Basin, Liard River Basin, Athabasca River Basin, and Peace River Basin represent the whole drainage area of the sub-basins, respectively (Fig. 1).

3. Data

3.1. Brightness temperature of SSM/I

SSM/I instruments on the US Defense Meteorological Satellite Program satellites have been providing continual monitoring of the Earth's surface since 1987. The SSM/I sensor has 7 channels including both horizontally and vertically-polarized channels at frequencies of 19.35, 37.0, and 85.5 GHz and a vertical polarization channel at 22.235 GHz. The SSM/I sensors can provide near global coverage at 25 km resolution every day except some small diamond-shaped areas near the equator and circular sectors of 2.4° latitude surrounding the north and south poles [1]. Ascending and descending orbit data are available every day. The present study uses daily SSM/I North Hemisphere EASE-Grid brightness temperature (TB) data at 25 km resolution from both ascending and descending orbits from 1988 to 2007 obtained from the NSIDC in Boulder, Colorado [ftp://sidads.colorado.edu/pub/DATASETS/].

3.2. MODIS snow products

MODIS, which has been flying on the Terra spacecraft since 18 December 1999, has 36 discrete, narrow spectral bands from approximately 0.4 to 14.4 μm. The spatial resolution of MODIS bands ranges from 250 m to 1000 m with a spectral resolution of 0.01 μm to 0.05 μm for different bands. MODIS snow cover products are mainly based on the SNOWMAP algorithm [13,19,20,24]. The snow maps are available at different resolutions and projections such as 500 m daily and 8-day data on a sinusoidal projection and 0.05°, 0.25° daily, 8-day, and monthly data on a latitude/longitude grid or the so-called climate-modeling grid (CMG). All snow maps are distributed through the NSIDC [http://nsidc.org]. In this paper, version 005 (V5) of MOD10A2 from 2001 to 2007, which are 8-day maximum snow cover extent with 500 m resolution, are used to validate recent SSM/I snow cover products.

3.3. River discharge and climatological data

Daily discharge data from 1988 to 2007 at the five gauges in the MRB (10LC014, drainage area (DA): 1,679,100 km^2), Peel River basin (10MC002, DA: 70,600 km^2), Liard River basin (10ED002, DA: 275,000 km^2), Athabasca River basin (07DA001, DA: 132,585 km^2), and Peace River basin (07KC001, DA: 293,000 km^2) are available from the Water Survey of Canada [http://www.wsc.ec.gc.ca/hydat/H2O/]. The discharge is divided by basin area to convert into runoff. To explore the relationships between snow distribution, streamflow, and climatology, the pentad precipitation and daily mean air temperature from 1987 to 2007 are downloaded from the National Centers for Environmental Prediction (NCEP) [http://www.cdc.noaa.gov/cdc/]. Although the exact accuracy of the NCEP precipitation and temperature fields is difficult to ascertain, the data have been shown to capture with accuracy the interannual variability in arctic regions [33,34]. The precipitation and air temperature data are on a global 2.5° latitude × 2.5° longitude grid; however, only the climatological fields for the grid points within the MRB are used to calculate the basin mean precipitation and air temperature.

4. Methods

4.1. SWE retrieval from SSM/I

The EC algorithm, which is a land cover sensitive algorithm to determine SWE based on the TB difference between the vertically-polarized 37 and 19 GHz channels of SSM/I, has been developed and evaluated over western Canada [8,9]. The SWE for an EASE-Grid cell is an area weighted average of the SWE calculated by the separate algorithms for each of four different land covers, which is expressed as:

$$SWE = F_O(SWE_O) + F_C(SWE_C) + F_D(SWE_D) + F_S(SWE_S) \quad (1)$$

where F_i is the fraction of land cover type for open (O), coniferous (C), deciduous (D), and sparse (S) forests and SWE_i is the SWE algorithm for each land cover type. The SWE algorithms for the four land cover classes for SSM/I are listed in Table 1 [8,9]. The 2004 MODIS International Geosphere–Biosphere Programme (IGBP) 1 km products [http://edcdaac.usgs.gov/] are used to calculate the land cover fractions for each EASE-Grid cell. The 17 IGBP land cover classes are reclassified into open, coniferous forest, deciduous forest, and sparse forest.

4.2. 25 km resolution snow cover maps from MOD10A2

To decrease the cloud coverage of MOD10A2, a spatial filter method is used to produce new snow cover maps, henceforth referred to as SF [39,40]. However, a single SSM/I SWE pixel (25 km) contains 2500 MOD10A2 pixels (500 m). Therefore, the SF products are reclassified into new snow cover maps with 25 km resolution in the following way: The MOD10A2 snow maps are reprojected into EASE-Grid Northern Hemisphere projection with ENVI/IDL software. For the 2500 pixels (500 m) of the SF product in a 25 km EASE-Grid of SSM/I, the EASE-Grid is classified as the majority of the classes of snow, no

Please cite this article as: Tong J, et al, Snow distribution from SSM/I and its relationships to the hydroclimatology of the Mackenzie River Basin, Canada, Adv Water Resour (2010), doi:10.1016/j.advwatres.2010.03.009

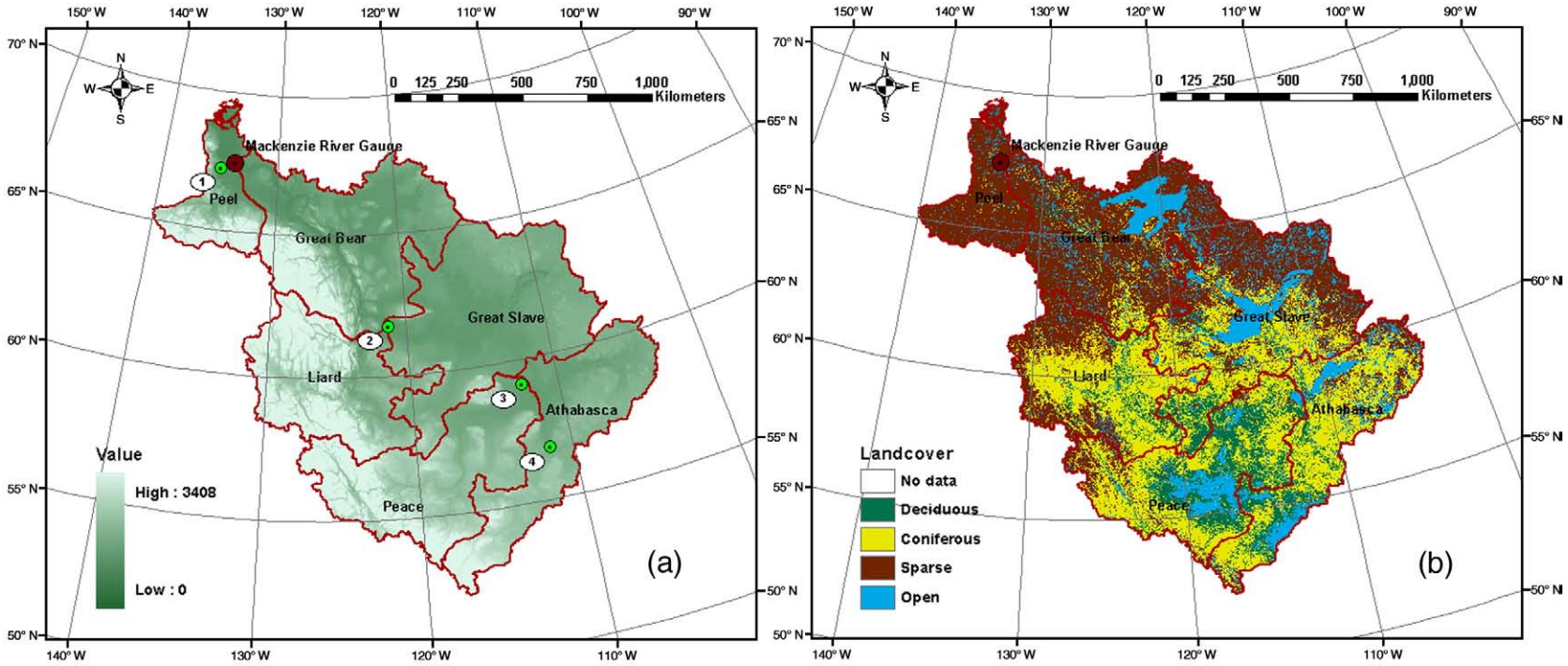

Fig. 1. Topographic (a) and land cover (b) map of the Mackenzie River Basin (MRB). The green circles with numbers 1, 2, 3, and 4 represent the river gauges at Peel River, Liard River, Peace River, and Athabasca River, respectively. The digital elevation model is from the Global Land One-kilometer Base Elevation (GLOBE) data set provided by the National Geophysical Data Center. The land cover type is from MODIS International Geosphere–Biosphere Programme (IGBP) 1 km land cover products. (For interpretation of the references to color in this figure legend, the reader is referred to the web version of this article.)

Table 1
Environment Canada SWE retrieval algorithms for different land cover types [8,9].

Land cover type	SSM/I SWE algorithm
Open	SWE = −20.7–2.59(37V–19V)
Coniferous forest	SWE = 16.81–1.96(37V–19V)
Deciduous forest	SWE = 33.5–1.97(37V–19V)
Sparse forest	SWE = −1.95–2.28(37V–19V)

Table 2
Confusion matrix for MODIS snow products and SSM/I.

SSM/I; MODIS	Snow	No snow
Snow	*a*	*b*
No snow	*c*	*d*

snow, or cloud among the 2500 pixels. Therefore, MOD10A2 8-day snow cover maps with 25 km resolution from 2001 to 2007 utilizing this version of the SF are considered as "ground truth" to evaluate those from SSM/I.

4.3. Comparison between the snow cover maps from SSM/I and SF products

Snow cover maps from SSM/I are produced based on the SWE that is retrieved from the EC algorithm. Owing to the heterogeneous nature of snow distributions in complex topography at the scale of the EASE-Grid pixel, the minimum threshold of SWE (referred to as k) from SSM/I to classify the pixel as snow or no snow is a critical problem to produce snow cover maps from this product. To determine the best threshold, various 8-day snow cover maps, which cover the same temporal scale as the MOD10A2 data, are produced based on different SWE thresholds from SSM/I. In every 8-day period, as long as SWE of a given pixel of one day is greater than the threshold, the pixel is classified as snow; otherwise, the pixel is classified as no snow. Therefore, for every given pixel, there are two different time series of snow condition, one from SSM/I and the other from the SF. The SF is taken as ground truth to evaluate the accuracy of the snow maps of SSM/I for every pixel according to the methods used by Pu et al. [31] and Parajka and Blöschl [30]. For a given pixel, there are four outcomes possible in comparing the SF with SSM/I (Table 2). The overall accuracy (OA) of SSM/I snow products is calculated through the entire period from:

$$Overall\ Accuracy = \frac{a+d}{a+b+c+d} \quad (2)$$

where terms a, b, c and d are defined in Table 2. All accuracies are based on the days when the SF snow products are not giving a classification as cloud. Then for every given threshold of SWE, the average OA of snow maps from SSM/I in every sub-basin is calculated based on the OA of every EASE-Grid pixel. Therefore, the threshold of SWE corresponding to the highest average OA for every sub-basin is determined as the final threshold of SWE to classify the EASE-Grid pixel as snow or no snow from SSM/I. The large water bodies (e.g., Great Slave Lake and Great Bear Lake) in the MRB are excluded in the comparison.

4.4. Comparison between the snow distribution, streamflow, and climatological data

SCE and SCF in this paper represent the total area of snow cover and percentage of snow cover at a given time in the whole MRB, respectively. The SCE, SCF, and SWE retrieved from SSM/I from 1988 to 2007 in the MRB are adopted to analyze the change of snow distribution in the last two decades. The correlation coefficients between SCF, mean SWE from SSM/I and streamflow of the MRB are calculated in the snow ablation season. To explore the relationship between SCF, runoff, and climate, $SCF_{50\%}$ is defined as the date at which the SCF attains 50% during each snow ablation season from 2 March (pentad 13) to 30 June (pentad 37), whereas the dates at which the normalized averaged SWE attains 50% of seasonal maximum values during snow the ablation season is denoted by $SWE_{50\%}$. The determination of $SCF_{50\%}$ and $SWE_{50\%}$ is easier and more accurate

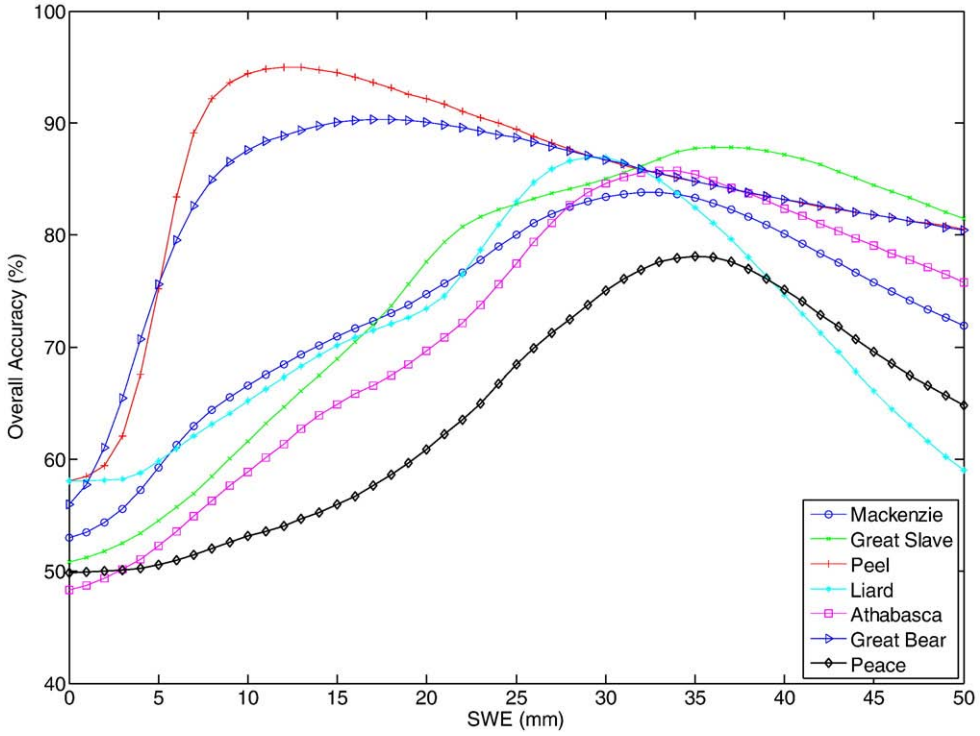

Fig. 2. The overall accuracy of snow cover maps based on different thresholds of SWE retrieved from SSM/I in various basins.

Please cite this article as: Tong J, et al, Snow distribution from SSM/I and its relationships to the hydroclimatology of the Mackenzie River Basin, Canada, Adv Water Resour (2010), doi:10.1016/j.advwatres.2010.03.009

Table 3
The thresholds of SWE with highest overall accuracy of snow cover maps from SSM/I in the different basins.

Basins	Mackenzie	Great Slave	Peel	Liard	Athabasca	Great Bear	Peace
Best thresholds (mm)	33	37	12	29	33	18	35

compared to the end date of SCF and SWE in the snow ablation seasons owing to the transient snowfall events in the early fall and in the late spring [5]. In addition, Tong et al. [40] have found significant relationships between $SCF_{50\%}$ and air temperature in a small catchment in western Canada. During snow ablation seasons, the corresponding average air temperatures for given periods are calculated. The periods are aggregated from the first date of 2 March to the given date. Then the Julian days of $SCF_{50\%}$ and $SWE_{50\%}$, which begin from the first day of every year, are compared with average air temperature and precipitation within different periods in the MRB. Statistical models are developed between various hydro-climatological quantities in the watersheds based on observed discharge and retrieved SCF and SWE from SSM/I from 1988 to 2007.

5. Results

5.1. Determination of thresholds k for snow cover products from SSM/I

Snow or no snow conditions for every SSM/I EASE-Grid pixel are determined according to different SWE thresholds ranging from 0 mm to 50 mm. The OAs of the pixels for the various thresholds are assessed with the corresponding MOD10A2 snow products that are considered here as ground truth. The average OAs for different sub-basins in the MRB with thresholds ranging from $k=0$ mm to 50 mm are shown in Fig. 2. The average OAs of 50% at $k=0$ mm are lowest in all the sub-basins. Then, the OAs increase to their highest values at near 90% for various thresholds in different sub-basins. The thresholds of the best OAs for different sub-basins are listed in Table 3. The Peel and Great Bear basins have substantially lower thresholds than the other basins. The land cover map of the MRB (Fig. 1) shows that these two basins are 94% and 80% covered by sparse forest or open area, respectively; however, the other basins are mainly covered by coniferous and deciduous forests, with these fractions ranging from 50% to 75%. Owing to the effects of vegetation on SWE retrieval from passive microwave remote sensing, the regions with greater forest cover require higher thresholds to be classified as snow based on SSM/I data.

Fig. 3 shows the averaged annual 8-day SCF for the MRB from 2001 to 2007 calculated from 8-day SF and SSM/I snow cover products based on the different thresholds, respectively. The "optimal" thresholds are the SWE number corresponding to the highest OAs in each sub-basin. The optimal case means the SCF is calculated according to the determined thresholds for different sub-basins. For thresholds 0 mm, 10 mm, 20 mm, and 30 mm, the SCFs of SSM/I are greater than those of the SF, nearing 100% SCF from January to March. The difference of SCFs between SSM/I and SF is likely caused by cloud coverage in the SF [40,47]. However, the SCFs of SSM/I based on thresholds 0 mm, 10 mm, and 20 mm, are much higher than SCFs of SF from March to December. Furthermore, the SCFs of SSM/I are about 20%, 40%, and 60% for thresholds 0 mm, 10 mm, and 20 mm, respectively, from July to September when the SCFs of SF are about 0%. However, the SCFs of SSM/I based on the thresholds of 40 mm and 50 mm are lower than SCFs of the SF throughout the whole year. The SCFs of SSM/I based on the optimal thresholds and 30 mm are closest to the SCFs of SF. However, compared with the SCFs of SF, SCFs of SSM/I based on optimal thresholds suggest about 40 days earlier snow accumulation than SCFs of SSM/I based on thresholds of 30 mm. All results indicate that the optimal thresholds are most suitable for classification of snow/no snow conditions in the MRB with an OA of about 90% compared to the SF. Therefore, all the SCFs of SSM/I are henceforth calculated according to the optimal thresholds.

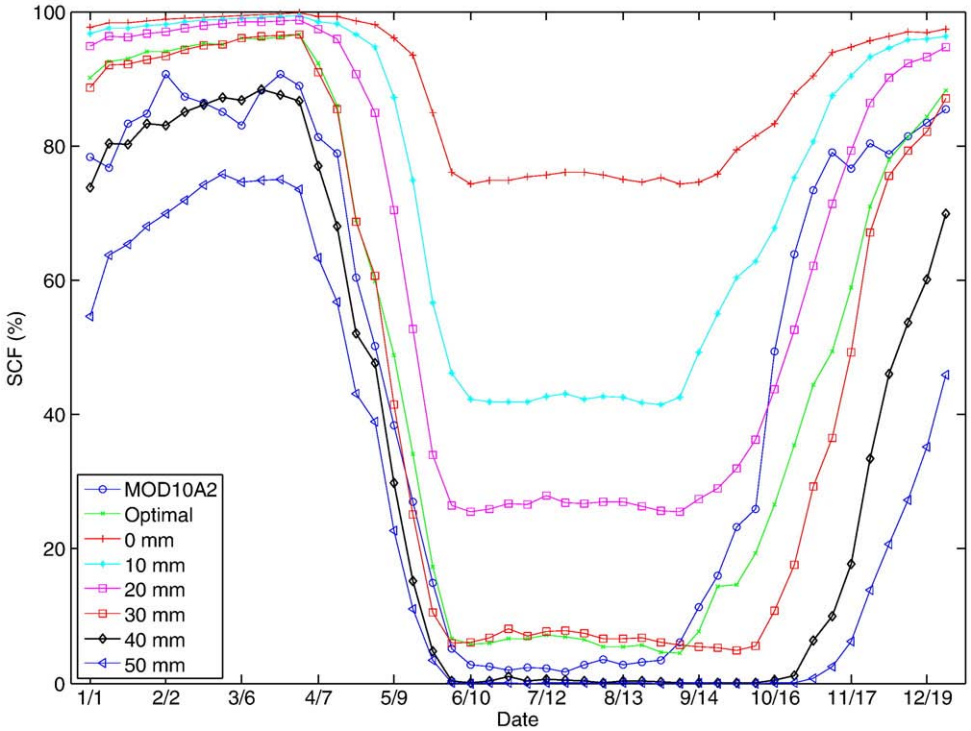

Fig. 3. The averaged eight-day annual cycle of SCF based on different thresholds of SWE from SSM/I and averaged eight-day annual cycle of SCF MOD10A2 from 2001 to 2007 in the Mackenzie River Basin.

Please cite this article as: Tong J, et al, Snow distribution from SSM/I and its relationships to the hydroclimatology of the Mackenzie River Basin, Canada, Adv Water Resour (2010), doi:10.1016/j.advwatres.2010.03.009

5.2. Distribution of SCF and SWE

The averaged pentad annual cycles of SCF and SWE based on SSM/I from 1988 to 2007 in the sub-basins of the MRB are shown in Fig. 4. Snow accumulation and ablation processes vary among different sub-basins. The beginning of the snow accumulation ranges from early September to mid-October. The Peel basin experiences the earliest snow accumulation, beginning around 3 September (pentad 50), and the Great Slave basin experiences the latest snow accumulation, commencing around 13 October (pentad 58). However, the averaged annual cycles of SCF and SWE show different processes of snow ablation. The beginning of the decrease in SCF ranges from early March to late April for the different basins. The Peace basin is the first to show a decrease of SCF, starting near 7 March (pentad 14), and the Peel basin is the latest to show a decrease of SCF, starting around 26 April (pentad 24). However, the decrease of SWE begins at around the same period near 7 March (pentad 14) for the various watersheds. Therefore, the snow accumulation season and snow ablation season are defined from 1 September to 30 November and from 1 March to 30 June, respectively. The higher latitude basins such as the Peel and Great Bear basins reach their highest SCF at about 100% and mean SWE of about 80 mm near 7 March (pentad 14), and the lower latitude basins such as the Peace and Athabasca basins reach their highest SCF of only about 90% and mean SWE near 50 mm on the same date (around 7 March or pentad 14).

5.3. Relationships between snow distribution and climatological conditions

Differences in snow accumulation and ablation processes among the six sub-basins are mainly due to their different air temperature and precipitation regimes. The Peel and Great Bear basins, which have the earliest snow accumulation and latest snow ablation processes, experience the lowest monthly mean air temperatures throughout the whole year. However, the Peace and Athabasca basins experience the highest monthly mean air temperatures resulting in the latest snow accumulation and earliest snow ablation (Fig. 5). The Peel basin is about 9.3 °C and 9.1 °C cooler than the Athabasca basin in March and November, respectively. The precipitation regime is also different across the six sub-basins (Fig. 5). During the snow accumulation season, the Athabasca basin has the lowest monthly mean precipitation, which combined with the highest temperature results in the least SCF and SWE. Although the monthly mean precipitation in the Peel and Great Bear basins is not the highest of the basins, it is at about the same level compared to the other sub-basins during the snow accumulation season. When this is combined with the much lower air temperatures, the Peel and Great Bear basins have the most seasonally accumulated SCF and SWE.

To quantify the relationships between snow ablation and air temperatures in the basins, the $SCF_{50\%}$ and $SWE_{50\%}$ from 1988 to 2007 in the sub-basins are calculated (Table 4). The average $SCF_{50\%}$ ranges from 18 April (Julian day 108) in the Peace basin to 23 May (Julian day 143) in the Peel basin. The average $SWE_{50\%}$ ranges from 21 April (Julian day 111) in the Athabasca basin to 8 May (Julian day 128) in the Peel basin. The correlation coefficients between $SCF_{50\%}$ and $SWE_{50\%}$ from SSM/I, mean air temperature within different periods, and monthly mean precipitation from January to December 1988–2007 are then calculated, respectively. Correlation coefficients between the $SCF_{50\%}$, $SWE_{50\%}$, and precipitation are always less than -0.1, demonstrating there is no significant relationship between them. However, there always exist significant negative correlation coefficients between $SCF_{50\%}$, $SWE_{50\%}$, and mean air temperatures from March to June, which indicates that higher temperatures result in faster snow ablation in both SCF and SWE. The maximum absolute values of negative correlation coefficients between $SCF_{50\%}$, $SWE_{50\%}$, and mean air temperatures always occur during the period beginning on 2 March and ending from 6 May to 30 June in different basins (Table 5). The maximum absolute values of negative correlation coefficients between $SCF_{50\%}$ and mean air temperatures range from 0.31 ($p<0.5$) to 0.72 ($p<0.001$) among the different sub-basins. The maximum absolute values of negative correlation coefficients between $SWE_{50\%}$ and mean air

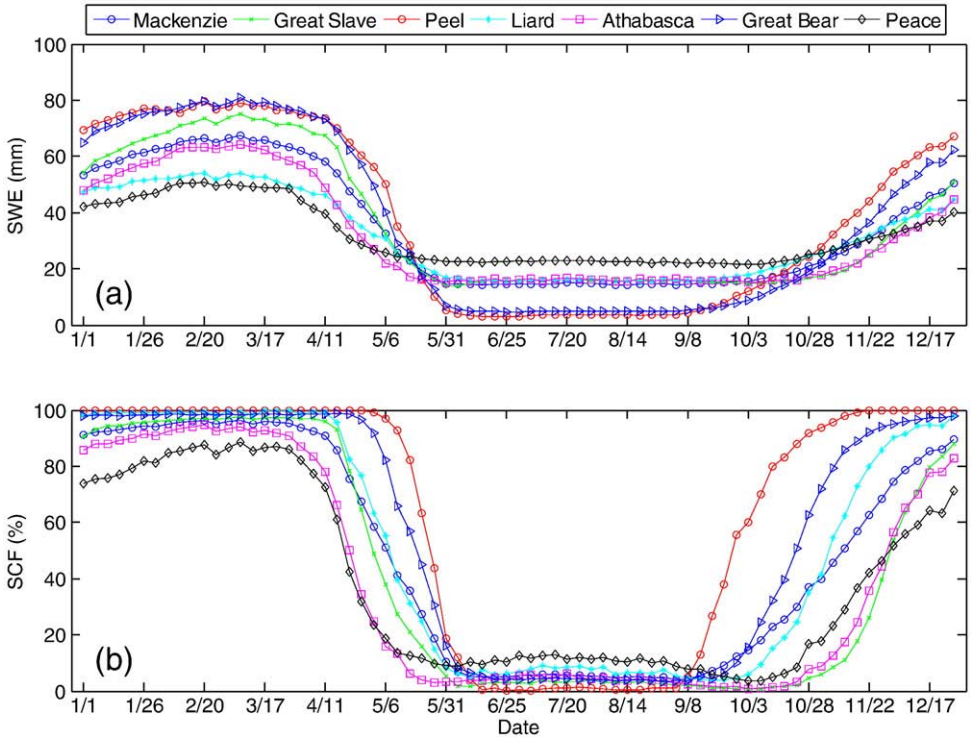

Fig. 4. The averaged pentad cycle of SWE (a) and SCF (b) retrieved from SSM/I from 1988 to 2007 in the different basins.

Please cite this article as: Tong J, et al, Snow distribution from SSM/I and its relationships to the hydroclimatology of the Mackenzie River Basin, Canada, Adv Water Resour (2010), doi:10.1016/j.advwatres.2010.03.009

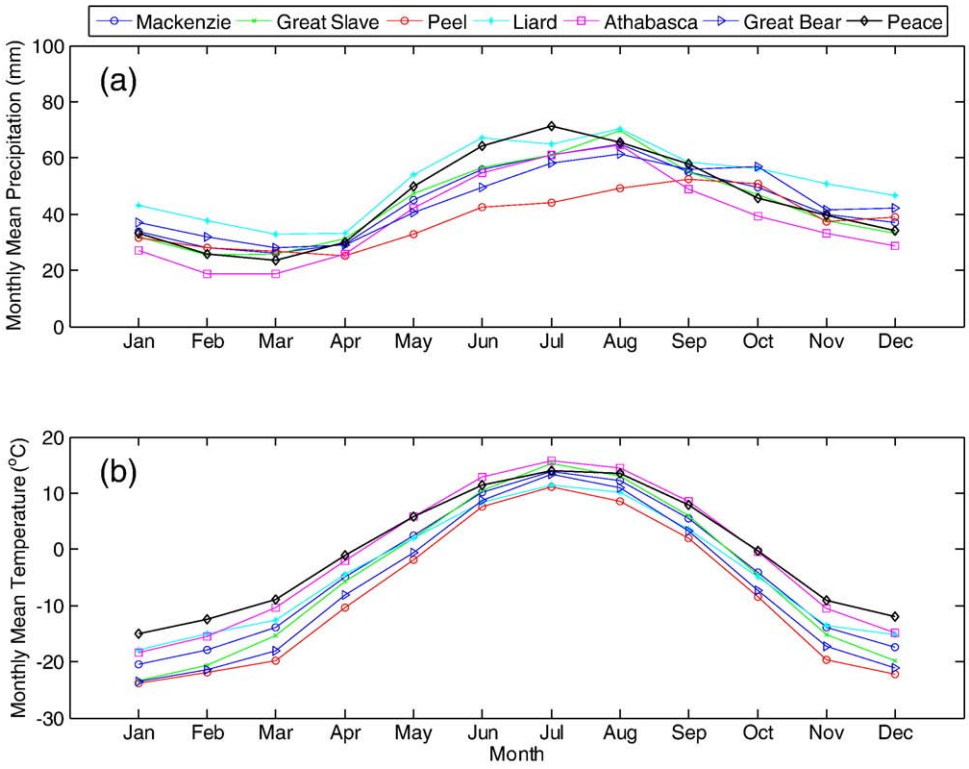

Fig. 5. Monthly mean precipitation (a) and monthly mean air temperature (b) based on the NCEP data from 1988 to 2007 in the different basins.

temperatures range from 0.22 ($p<0.5$) to 0.66 ($p<0.01$) among different sub-basins. In all the sub-basins, the $SCF_{50\%}$ exhibits more significant correlation coefficients with mean air temperature than $SWE_{50\%}$ does. For the Athabasca basin, $SCF_{50\%}$ and $SWE_{50\%}$ are plotted against mean air temperatures in the given period during the snow ablation seasons from 1988 to 2007, and the regression lines and correlation coefficients are shown in Fig. 6 (for brevity, similar figures for the other sub-basins are not shown). It demonstrates strong linear relationships between $SCF_{50\%}$, $SWE_{50\%}$, and mean air temperatures. The regression equations between $SCF_{50\%}$, $SWE_{50\%}$, and mean air temperatures in all basins, which are listed in Table 6, can thus be adopted to reliably predict the snow ablation process in the basins.

5.4. Relationships between snow distribution and river runoff

The averaged annual cycle of runoff at the MR gauge and the averaged annual cycle of SCF and SWE from SSM/I from 1988 to 2007 in the MRB are shown in Fig. 7. It shows that the runoff begins to increase around 21 April (pentad 23) to reach its peak value near 26 May (pentad 30). Then the runoff decreases to its lowest value around 2 December (pentad 68). The trend in runoff is opposite to the trend of the SCF and SWE. The high rates of increase in runoff occur from 21 April (pentad 23) to 26 May (pentad 30) when the high snow ablation rates of SCF and SWE occur as well (for brevity, similar figures for other sub-basins are not shown here).

Table 4
Annual average Julian days of $SWE_{50\%}$ and $SCF_{50\%}$ from 1988–2007 in different basins.

Basins	Mackenzie	Great Slave	Peel	Liard	Athabasca	Great Bear	Peace	Standard deviations
Julian day of $SWE_{50\%}$	121	119	128	124	111	122	120	5
Julian day of $SCF_{50\%}$	125	120	143	127	111	136	108	12

The runoff in the basins is highly related to the SCF with correlation coefficients of −0.85, −0.69, −0.81, −0.77, and −0.52 and SWE with correlation coefficients of −0.79, −0.67, −0.78, −0.73, and −0.52, for the MRB, Peel River basin, Liard River basin, Athabasca River basin, and Peace River basin, respectively ($p<0.001$ for all correlation coefficients).

The lagged correlation coefficients between SCF, SWE and runoff during snow ablation seasons are also calculated based on daily SCF and SWE from SSM/I and runoff (Fig. 8). The absolute values of negative lagged correlation coefficients between SCF, SWE, and runoff reach a maximum ranging from 0.52 ($p<0.001$) to 0.87 ($p<0.001$) at 0–5 lagged days for different basins. To determine the runoff based on SCF and SWE, regression models are developed between the pentad SCF, SWE, and runoff during the snow ablation seasons, respectively. Scatter plots and regression equations between SCF, SWE, and runoff in the MRB are shown in Fig. 9 and the corresponding regression

Table 5
The date of the maximum absolute values of negative correlation coefficients between $SWE_{50\%}$, $SCF_{50\%}$, and mean air temperatures, the corresponding correlation coefficients, and the significant level.

		Date	Correlation coefficients	Significant level ($p<$)
Mackenzie	SWE	6/20	−0.37	0.1
	SCF	6/15	−0.54	0.01
Great Slave	SWE	5/26	−0.48	0.05
	SCF	5/31	−0.53	0.02
Peel	SWE	6/10	−0.30	0.5
	SCF	6/10	−0.43	0.05
Liard	SWE	6/30	−0.32	0.5
	SCF	5/11	−0.36	0.1
Athabasca	SWE	5/21	−0.66	0.01
	SCF	5/11	−0.72	0.001
Great Bear	SWE	6/10	−0.44	0.05
	SCF	6/20	−0.45	0.05
Peace	SWE	5/6	−0.23	0.5
	SCF	5/16	−0.31	0.5

Please cite this article as: Tong J, et al, Snow distribution from SSM/I and its relationships to the hydroclimatology of the Mackenzie River Basin, Canada, Adv Water Resour (2010), doi:10.1016/j.advwatres.2010.03.009

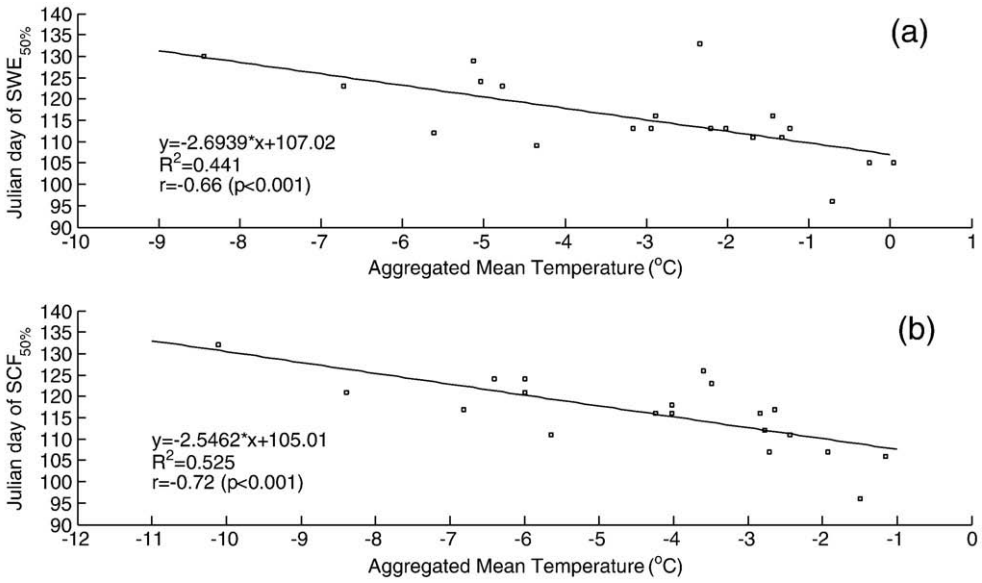

Fig. 6. Scatter plots between mean air temperature from 2 March to 21 May or 11 May and Julian day of $SWE_{50\%}$ (a) and $SCF_{50\%}$ (b) during snow ablation seasons from 1988 to 2007 in the Athabasca sub-basin.

equations are listed in Table 7. The results show strong relationships between SCF, SWE, and runoff for all the basins. The linear function shows the best regression equation between SCF and runoff, while a power function gives the best regression equation between SWE and runoff for all the basins. Comparing the SCF to discharge, the MRB has the highest coefficient of determination, $R^2 = 0.79$ ($p < 0.001$), while the Peel River basin has the lowest coefficient of determination, $R^2 = 0.21$ ($p < 0.001$). Comparing the SWE to discharge, the MRB has the best regression equations with $R^2 = 0.87$ ($p < 0.001$), while the Peace River basin has the regression equations with the lowest $R^2 = 0.36$ ($p < 0.001$).

6. Concluding discussion

This study applies the long-term microwave remotely sensed data from SSM/I to investigate the relationships between SCF, SWE, and the hydroclimatology of the MRB, Canada. The SWE is retrieved based on the land cover sensitive EC algorithm with a maximum error of 30 mm compared to ground-based observations in the MRB [8]. The MODIS 8-day snow maps are used to determine the threshold for SWE to classify the ground as snow or no snow. All the results show that the thresholds of SWE from SSM/I vary in different sub-basins and there exist significant relationships between snow ablation processes, the meteorology, and the hydrologic regime of the MRB.

Compared to the MODIS 8-day snow maps, the accuracy of the SCF from SWE of SSM/I ranges from about 50% to 90% based on different thresholds of SWE in the various sub-basins. The six main sub-basins of the MRB reach their maximum accuracy of the SCF at different thresholds. The Peel and Great Bear basins have lower thresholds and higher accuracy than the other basins owing to their flat terrain and sparse vegetation. The thresholds of SWE with highest accuracy of SCF at different sub-basins are combined as the optimal thresholds for the MRB, which has a 90% accuracy of SCF. The averaged annual cycle of SCF from SSM/I based on these optimal thresholds matches well the one derived from MODIS eight-day snow maps. Compared to the MODIS 8-day products, the new snow maps from SSM/I avoid degradation by cloud cover, which can be persistent in the Arctic. Therefore, daily cloud free snow maps inferred from SSM/I using the optimal thresholds of SWE are considered reliable. Furthermore, higher temporal resolutions of the cloud free snow maps will improve our future understanding of snow hydrology processes.

To quantify the influence of meteorological conditions on snow ablation processes, the 1988–2007 $SWE_{50\%}$, $SCF_{50\%}$, and mean air temperature and precipitation are compared in each sub-basin. There always exists a significant negative correlation between $SCF_{50\%}$, $SWE_{50\%}$, and mean air temperatures from March to June, which indicates that snow ablation processes are strongly modulated by the air temperature in the basins. The maximum absolute values of negative correlation coefficients between $SCF_{50\%}$, $SWE_{50\%}$, and mean air temperatures, which range from 0.22 ($p < 0.5$) to 0.72 ($p < 0.001$), always occur beginning from 2 March and ending from 6 May to 30 June for different sub-basins. The absolute values of lagged correlation coefficients between SCF, SWE, and discharge reach their maximum lag times between 0 and 5 days for different sub-basins. All the correlation relationships between SCF from SSM/I and runoff are stronger than SWE from SSM/I and runoff owing to the poor performance of SSM/I when the snow depth is higher than 1 m.

The results of this paper demonstrate that the SSM/I data and the EC SWE algorithm are able to yield the relationships between snow distribution and runoff in large northern watersheds, especially during early snow ablation seasons. The validation of the SCF from SSM/I based on the MODIS snow maps indicates that single thresholds for determining snow cover from SSM/I are not suitable in large northern

Table 6
The regression equations between mean air temperature (x) and Julian day of $SWE_{50\%}$ (y) and $SCF_{50\%}$ (y).

	$SWE_{50\%}$	$SCF_{50\%}$
Mackenzie	$y = -1.7378x + 121.5$ $R^2 = 0.14$	$y = -2.2207x + 122.89$ $R^2 = 0.30$
Great Slave	$y = -2.1747x + 110.08$ $R^2 = 0.23$	$y = -2.2869x + 111.45$ $R^2 = 0.28$
Peel	$y = -1.4596x + 119.55$ $R^2 = 0.09$	$y = -1.7381x + 132.32$ $R^2 = 0.19$
Liard	$y = -1.9854x + 125.95$ $R^2 = 0.10$	$y = -1.2541x + 123.57$ $R^2 = 0.13$
Athabasca	$y = -2.6939x + 107.02$ $R^2 = 0.44$	$y = -2.5462x + 105.01$ $R^2 = 0.53$
Great Bear	$y = -1.9876x + 113.59$ $R^2 = 0.20$	$y = -1.9836x + 130.5$ $R^2 = 0.20$
Peace	$y = -0.3704x + 119.54$ $R^2 = 0.05$	$y = -3.2098x + 103.25$ $R^2 = 0.11$

Please cite this article as: Tong J, et al, Snow distribution from SSM/I and its relationships to the hydroclimatology of the Mackenzie River Basin, Canada, Adv Water Resour (2010), doi:10.1016/j.advwatres.2010.03.009

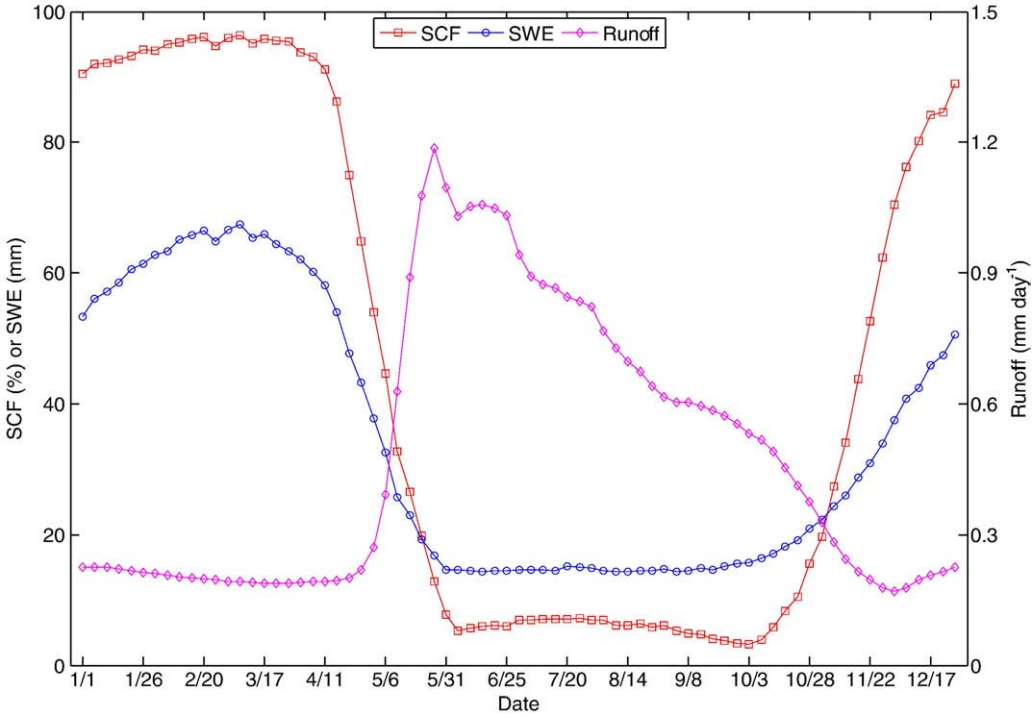

Fig. 7. The averaged pentad SCF and SWE from SSM/I and runoff from 1988 to 2007 in the Mackenzie River Basin.

watersheds. The new SCF products from SSM/I perform better than SWE from SSM/I to analyze the relationships with the regional hydroclimatology. Since the peak runoff almost occurs during the end of snow ablation seasons when the hydrologic systems are most sensitive to the liquid precipitation due to the warmer air temperature [14], precipitation should also be included into snow–precipitation–runoff model to better predict the peak runoff at this time.

Compared to previous work in large northern watersheds [41,46], this study is novel in developing new snow maps based on the SSM/I SWE. In addition, we also find that a single threshold such as 1 mm of

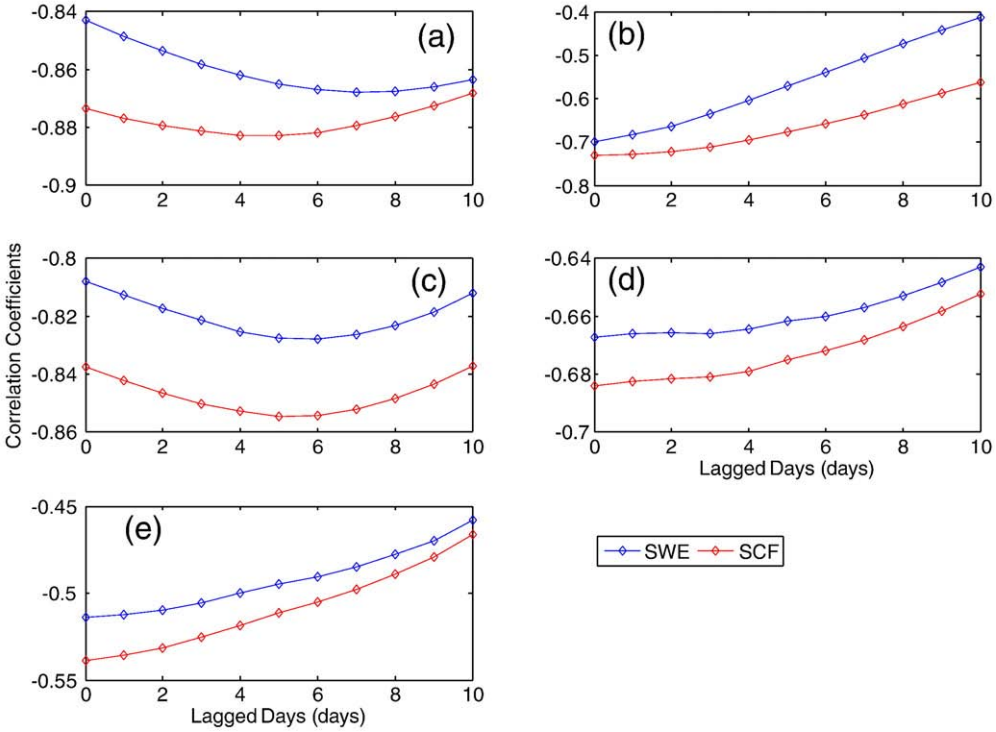

Fig. 8. The lagged correlation coefficients between SCF, SWE, and runoff during snow ablation seasons from 1988 to 2007 in the a) Mackenzie River Basin, b) Peel River Basin, c) Liard River Basin, d) Athabasca River Basin, and e) Peace River Basin.

Please cite this article as: Tong J, et al, Snow distribution from SSM/I and its relationships to the hydroclimatology of the Mackenzie River Basin, Canada, Adv Water Resour (2010), doi:10.1016/j.advwatres.2010.03.009

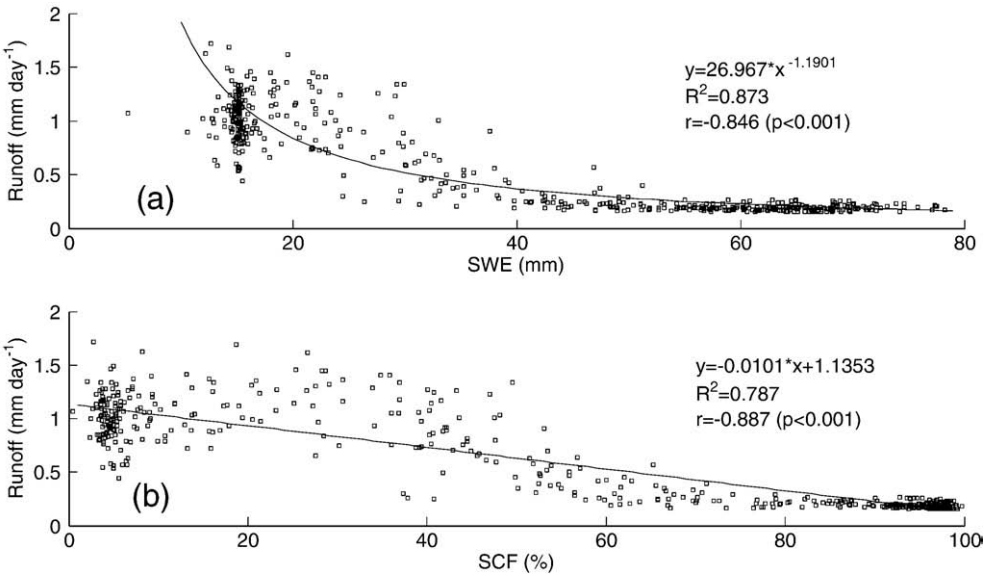

Fig. 9. Scatter plots between runoff and SWE (a) and SCF (b) during snow ablation seasons from 1988 to 2007 in the Mackenzie River Basin.

SWE is not suitable for the new snow cover maps in large forested, mountainous watersheds and we suggest that an optimal threshold improves the correlations between snow cover and streamflow. In this study, we mainly focused on the major surface hydrological processes such as snow distribution, precipitation, streamflow and air temperature in northern watersheds. Although the freeze–thaw cycle of lakes in the area will also affect hydrological processes, it works more importantly at annual or decade time scales and is beyond the scope of this study. The MRB is one of the major watersheds that provides freshwater to the Arctic Ocean. The approach developed in this work to produce new snow cover maps and to quantify snowmelt-streamflow processes in the MRB will therefore improve our understanding of cold regions hydrology and the freshwater budget of the Arctic Ocean.

Acknowledgments

Supported by the Natural Sciences and Engineering Research Council (NSERC) of Canada, the Canada Research Chair program (S. Déry), and an NSERC Discovery Grant (C. Derksen). Comments by Dr. Juraj Parajka (Vienna University of Technology) and two anonymous referees greatly improved the paper.

Table 7
The regression equations between remotely sensed SCF (x) or SWE (x) and runoff (y) in the basins. The correlation coefficients between SCF, SWE, and runoff are shown in Fig. 8.

	SCF	SWE
Mackenzie	$y=-0.0101x+1.1353$ $R^2=0.79$	$y=26.967x^{-1.1901}$ $R^2=0.87$
Peel	$y=-0.0178x+2.5559$ $R^2=0.21$	$y=7.6242x^{-0.8597}$ $R^2=0.62$
Liard	$y=-0.0216x+2.3679$ $R^2=0.76$	$y=869.37x^{-2.151}$ $R^2=0.79$
Athabasca	$y=-0.0064x+0.7595$ $R^2=0.50$	$y=17.517x^{-1.1713}$ $R^2=0.66$
Peace	$y=-0.0058x+1.0328$ $R^2=0.27$	$y=10.92x^{-0.7971}$ $R^2=0.36$

References

[1] Armstrong R, Brodzik M. An Earth-gridded SSM/I data set for cryospheric studies and global change monitoring. Adv Space Res 1995;16(10):155–63.
[2] Barnett TP, Adam JC, Lettenmaier DP. Potential impacts of a warming climate on water availability in snow-dominated regions. Nature 2005;438:303–9, doi:10.1038/nature04141.
[3] Brown RD. Northern hemisphere snow cover variability and change 1915–1997. J Clim 2000;13:2339–55.
[4] Brown RD. Snow cover variability and trends in the Mackenzie Basin, 1945–2005. In: di Cenzo P, editor. Final Report of the Mackenzie GEWEX Study (MAGS): Proceeding of the Final (11th) Annual Scientific Meeting; 2006. p. 319–37.
[5] Brown R, Derksen C, Wang L. Assessment of spring snow cover duration variability over northern Canada from satellite datasets. Remote Sens Environ 2007;111(2):367–681, doi:10.1016/j.rse.2006.09.035.
[6] Chang ATC, Foster JL, Hall DK. Nimbus-7 SMMR derived global snow cover parameters. Ann Glaciol 1987;9:39–44.
[7] Derksen C. The contribution of AMSR-E 18.7 and 10.7 GHz measurements to improved boreal forest snow water equivalent retrievals. Remote Sens Environ 2008;112:2701–10.
[8] Derksen C, Walker A, Goodison B. A comparison of 18 winter seasons of in situ and passive microwave-derived snow water equivalent estimates in Western Canada. Remote Sens Environ 2003;88:271–82.
[9] Derksen C, Walker A, Goodison B. Evaluation of passive microwave snow water equivalent retrievals across the boreal forest/tundra transition of western Canada. Remote Sens Environ 2005;96:315–27.
[10] Déry SJ, Brown RD. Recent Northern Hemisphere snow cover extent trends and implications for the snow-albedo feedback. Geophys Res Lett 2007;34:L22504, doi:10.1029/2007GL031474.
[11] Déry SJ, Crow WT, Stieglitz M, Wood EF. Modeling snow-cover heterogeneity over complex Arctic terrain for regional and global climate models. J Hydrometeorol 2004;5:33–48.
[12] Déry SJ, Salomonson VV, Stieglitz M, Hall DK, Appel I. An approach to using snow areal depletion curves inferred from MODIS and its application to land surface modelling in Alaska. Hydrol Proc 2005;19:2755–74, doi:10.1002/hyp.5784.
[13] Dozier J. Spectral signature of alpine snow cover from the Landsat Thematic Mapper. Remote Sens Environ 1989;28:9–22.
[14] Dyer J. Snow depth and streamflow relationships in large North American watersheds. J Geophys Res 2008;113(D18113), doi:10.1029/2008JD010031.
[15] Goodison BE, Walker AE. Canadian development and use of snow cover information from passive microwave satellite data. In: Choudhury BJ, et al, editor. Passive Microwave Remote Sensing of Land–Atmosphere Interactions. Proceedings of the ESA/NASA International Workshop. Zeist, Netherlands: VSP; 1995. p. 245–62.
[16] Groisman PY, Knight RW, Karl TR, Easterling DR, Sun B, Lawrimore JH. Contemporary changes of the hydrological cycle over the contiguous United States: Trends derived from in situ observations. J Hydrometeorol 2004;5:64–85.
[17] Hall DK, Foster JL, Verbyla DL, Klein AG, Benson CS. Assessment of snow-cover mapping accuracy in a variety of vegetation-cover densities in central Alaska. Remote Sens Environ 1998;66(2):129–37.
[18] Hall DK, Riggs GA. Accuracy assessment of the MODIS snow-cover products. Hydrol Proc 2007;21(12):1534–47.

Please cite this article as: Tong J, et al, Snow distribution from SSM/I and its relationships to the hydroclimatology of the Mackenzie River Basin, Canada, Adv Water Resour (2010), doi:10.1016/j.advwatres.2010.03.009

[19] Hall DK, Riggs GA, Salomonson VV. Development of methods for mapping global snow cover using moderate resolution imaging spectroradiometer data. Remote Sens Environ 1995;54(2):127–40.
[20] Hall DK, Riggs GA, Salomonson VV, Digirolamo NE, Bayr KJ. MODIS snow-cover products. Remote Sens Environ 2002;83:181–94.
[21] Jain S, Lall U. Magnitude and timing of annual maximum floods: trends and large-scale climatic associations for the Blacksmith Fork River, Utah. Water Resour Res 2000;36(12):3641–51.
[22] Kelly R, Chang ATC. Development of a passive microwave global snow depth retrieval algorithm for Special Sensor Microwave Imager (SSM/I) and Advanced Microwave Scanning Radiometer-EOS (AMSR-E) data. Radio Sci 2003;38(4):8076, doi:10.1029/2002RS002648.
[23] Klein GA, Barnett AC. Validation of daily MODIS snow cover maps of Upper Rio Grande River Basin for the 2000–2001 snow year. Remote Sens Environ 2003;86:162–76.
[24] Klein GA, Hall DK, Riggs GA. Improving snow cover mapping in forests through the use of a canopy reflectance model. Hydrol Proc 1998;12:1723–44.
[25] Massom R. Satellite remote sensing of polar snow and ice: present status and future direction. Polar Rec 1995;31(177):99–114.
[26] Maurer PE, Rhoads JD, Dubayah RO, Lettenmaier DP. Evaluation of snow-covered area data product from MODIS. Hydrol Proc 2003;17:59–71, doi:10.1002/hyp.1193.
[27] Mote PW. Climate-driven variability and trends in mountain snowpack in western North America. J Clim 2006;19(23):6209–20.
[28] Mote PW, Hamlet AF, Clark MP, Lettenmaier DP. Declining mountain snowpack in western North America. Bull Amer Meteorol Soc 2005;86:39–49, doi:10.1175/BAMS-86-1-39.
[29] Parajka J, Blöschl G. Validation of MODIS snow cover images over Austria. Hydrol Earth Syst Sci 2006;10:679–89.
[30] Parajka J, Blöschl G. Spatio-temporal combination of MODIS images-potential for snow cover mapping. Water Resour Res 2008;44:W03406, doi:10.1029/2007WR006204.
[31] Pu Z, Xu L, Salomonson VV. MODIS/Terra observed seasonal variations of snow cover over the Tibetan Plateau. Geophys Res Lett 2007;34:L06706, doi:10.1029/2007GL029262.
[32] Schmugge JT, Kustas WP, Ritchie JC, Jackson TJ, Rango A. Remote sensing in hydrology. Adv Water Resour 2002;25:1367–85.
[33] Serreze M, Hurst C. Representation of mean Arctic precipitation from NCEP–NCAR and ERA reanalyses. J Clim 2000;13:182–201.
[34] Simmons AJ, Jones PD, Bechtold VC, Beljaars ACM, Kallberg PW, Saarinen S, et al. Comparison of trends and low-frequency variability in CRU, ERA-40, and NCEP/NCAR analyses of surface air temperature. J Geophys Res 2004;109:D24115, doi:10.1029/2004JD005306.
[35] Stewart IT, Cayan DR, Dettinger MD. Changes towards earlier streamflow timing across western North America. J Clim 2005;18:1136–55.
[36] Stieglitz M, Déry SJ, Romanovsky VE, Osterkamp TE. The role of snow cover in the warming of arctic permafrost. Geophys Res Lett 2003;30(13):1721, doi:10.1029/2003GL017337.
[37] Stone RS, Dutton EG, Harris JM, Longenecker D. Earlier spring snowmelt in northern Alaska as an indicator of climate change. J Geophys Res 2002;107(D10), doi:10.1029/2000JD000286.
[38] Tedesco M, Pulliainen J, Takala M, Hallikainen M, Pampaloni P. Artificial neural network-based techniques for the retrieval of SWE and snow depth from SSM/I data. Remote Sens Environ 2004;90:76–85.
[39] Tong J, Déry SJ, Jackson PL. Topographic control of snow distribution in an alpine watershed of western Canada inferred from spatially-filtered MODIS snow products. Hydrol Earth Syst Sci 2009;13:319–26.
[40] Tong J, Déry SJ, Jackson PL. Interrelationships between MODIS/Terra remotely sensed snow cover and the hydrometeorology of the Quesnel River Basin, British Columbia, Canada. Hydrol Earth Syst Sci 2009;13:1439–52.
[41] Walker A, Silis A. Snow cover variations over the Mackenzie river basin from SSM/I passive microwave satellite data. Ann Glaciol 2002;34:8–14.
[42] Wang LB, Sharp M, Brown R, Derksen C, Rivard B. Evaluation of spring snow covered area depletion in the Canadian Arctic from NOAA snow charts. Remote Sens Environ 2005;95:453–63.
[43] Wang X, Xie H, Liang T, Huang X. Comparison and validation of MODIS standard and new combination of Terra and Aqua snow cover products in northern Xinjiang, China. Hydrol Proc 2009;23(3):419–29, doi:10.1001/hyp.7151.
[44] Yang D, Robinson D, Zhao Y, Estilow T, Ye B. Streamflow response to seasonal snow cover extent changes in large Siberian watersheds. J Geophys Res 2003;108(D18):4578, doi:10.1029/2002JD003149.
[45] Yang D, Zhao Y, Armstrong R, Robinson D. Streamflow response to seasonal snow cover mass changes over large Siberian watersheds. J Geophys Res 2007;112:F02S22, doi:10.1029/2006JF000518.
[46] Yang D, Zhao Y, Armstrong R, Robinson D. Yukon river streamflow response to seasonal snow cover changes. Hydrol Proc 2009;23:109–21.
[47] Zhou X, Xie H, Hendrickx MH. Statistical evaluation of remotely sensed snow-cover products with constraints from streamflow and SNOTEL measurements. Remote Sens Environ 2005;94:214–31.

Please cite this article as: Tong J, et al, Snow distribution from SSM/I and its relationships to the hydroclimatology of the Mackenzie River Basin, Canada, Adv Water Resour (2010), doi:10.1016/j.advwatres.2010.03.009